ACS POLYMERS Au
AN OPEN ACCESS JOURNAL OF THE AMERICAN CHEMICAL SOCIETY

pubs.acs.org/polymerau

Article

Stabilizing Polymer Coatings Alter the Protein Corona of DNA Origami and Can Be Engineered to Bias the Cellular Uptake

Published as part of the ACS Polymers Au virtual special issue "2023 Rising Stars".

Hugo J. Rodríguez-Franco, Jorieke Weiden, and Maartje M. C. Bastings*

Cite This: *ACS Polym. Au* 2023, 3, 344−353

Read Online

ACCESS | Metrics & More | Article Recommendations | Supporting Information

ABSTRACT: With DNA-based nanomaterials being designed for applications in cellular environments, the need arises to accurately understand their surface interactions toward biological targets. As for any material exposed to protein-rich cell culture conditions, a protein corona will establish around DNA nanoparticles, potentially altering the a-priori designed particle function. Here, we first set out to identify the protein corona around DNA origami nanomaterials, taking into account the application of stabilizing block co-polymer coatings (oligolysine-1kPEG or oligolysine-5kPEG) widely used to ensure particle integrity. By implementing a label-free methodology, the distinct polymer coating conditions show unique protein profiles, predominantly defined by differences in the molecular weight and isoelectric point of the adsorbed proteins. Interestingly, none of the applied coatings reduced the diversity of the proteins detected within the specific coronae. We then biased the protein corona through pre-incubation with selected proteins and show significant changes in the cell uptake. Our study contributes to a deeper understanding of the complex interplay between DNA nanomaterials, proteins, and cells at the bio-interface.

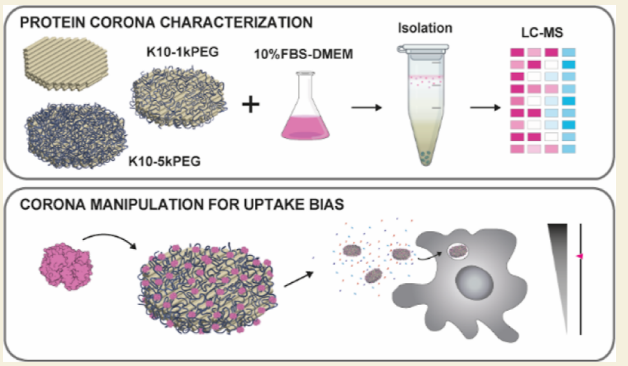

KEYWORDS: *protein corona, polymer coating, DNA nanomaterials, DNA origami, cellular uptake*

INTRODUCTION

The use of nanomaterials at biological interfaces typically implies their exposure to complex milieus of extracellular proteins, which quickly adsorb onto the material surface and form a corona.[1,2] Such corona is known to have a multi-layered structure, commonly differentiating an inner "hard corona", composed of proteins tightly bound to the nanoparticle surface, and an outer "soft corona" of highly dynamic nature, constituted by loosely bound, lower affinity proteins.[3] These non-specific protein coatings may alter the shape, size, and surface characteristics of nanomaterials, endowing them with a completely new biological identity that impacts their interface interactions and resulting biological response.[4] In particular, the protein corona has been proven to dictate nanomaterial toxicity, colloidal stability, interaction with the cellular membrane, cellular uptake, internal trafficking, targeting, and biodistribution.[5−8]

DNA origami nanoparticles (DONs), compact nanostructures created from the controlled self-assembly of long DNA scaffolds with hundreds of short synthetic DNA polymer "staples", have gained substantial interest as bioengineering tools due to their programmability, uniformity, and spatial addressability to present a wide variety of biomolecules in a controlled manner.[9] In order to fully exploit the potential of DONs in biological systems, a detailed characterization of their protein corona is paramount. Several studies have analyzed the proteomic profile of coronae adsorbed onto DNA-hybrid nanomaterials after incubation in human or mouse serum, while only one study has reported the proteomic composition of the corona formed around fully DNA-based nanoparticles, including DONs, when incubated in 55% human serum.[10−13] However, despite the extensive arrays of in vitro studies where these nanoparticles are applied at the cell interface, characterization of DON protein corona in standard cell culture conditions has not been performed so far.

Compact DONs rarely preserve their integrity when placed in biological contexts, predominantly challenged by nucleases and low cationic salt concentrations.[14] A highly effective and commonly used solution is the stabilization of DONs with a protective oligolysine-poly-ethylene glycol (PEG) polymeric coating.[15] Interestingly, PEGylation became the gold standard

Received: April 1, 2023
Revised: May 18, 2023
Accepted: May 22, 2023
Published: June 7, 2023

https://doi.org/10.1021/acspolymersau.3c00009
ACS Polym. Au 2023, 3, 344−353

technique to suppress protein adsorption and endow nanoparticles with stealth-like properties by fine-tuning the polymer length and grafting density.[16] However, recent reports suggested that the stealth effect observed on PEGylated nanoparticles is due to the preferential adsorption of certain proteins rather than to the complete suppression of corona formation, raising the interest to identify the specific proteins present on PEGylated bio-surfaces.[17] Despite the fact that the application of the stabilizing oligolysine-PEG coating might drastically change the profile of protein adsorption onto DONs,[18] its influence has never been characterized.

In addition to analyzing the non-specific adsorption of proteins on DNA nanoparticles, the controlled formation of protein coronae around DONs provides an interesting avenue to modulate nanoparticle behavior. A specific corona can be grafted onto DNA-based nanoparticles via direct electrostatic interactions or through intermediate compounds able to chemically and/or physically bridge proteins and DNA. Such approaches to engineer a customized protein corona have been successfully applied in fine-tuning colloidal and structural stability of DNA nanomaterials,[19−22] as well as their cellular uptake or targeting.[21−25] When proteins with an important role in promoting (opsonins) or discouraging (dysopsonins) uptake by phagocytic cells are used, the cellular uptake of nanoparticles can be modulated.[26−28] Here, we first analyze the effect of different stabilizing oligolysine-PEG polymer coatings on the protein corona composition of DONs when subjected to standard cell culture conditions and subsequently bias corona formation to influence the particle uptake by macrophages.

MATERIALS AND METHODS

DON Synthesis and Purification

The p7560 DNA scaffold was bought from Tilibit, and sequence-specific DNA staple strands, as previously published,[29] were purchased from Integrated DNA Technologies (IDTs). DONs were synthesized by mixing 10 nM of the p7560 scaffold with a 10-fold excess of non-modified staples strands and five-fold excess of Cy5-functionalized strands in 1× folding buffer (5 mM Tris (Merck), 1 mM EDTA (PanReac AppliChem), 5 mM NaCl (Sigma-Aldrich), and 18 mM $MgCl_2$ (Sigma-Aldrich), pH 8.0) in a total volume of 50 μL. Folding was performed using a thermal annealing ramp in a thermocycler (Biometra TRIO Analytik Jena) (80 °C for 5 min, 60 to 20 °C at −1 °C per hour). DONs were subsequently purified from the excess of staple strands and concentrated through PEG precipitation. In brief, the annealed solutions were mixed in a 1:1 (v/v) ratio with 2× PEG precipitation buffer (15% PEG8000—Sigma-Aldrich, 0.5 M NaCl, 5 mM Tris, 1 mM EDTA, and 18 mM $MgCl_2$), incubated at room temperature for 30 min and centrifuged at 16,000 rcf for 40 min at 20 °C. The supernatant was then removed, and the pelleted DONs were resuspended in 1× folding buffer by an overnight incubation at room temperature. The final stock concentration (40 nM) was measured with a NanoDrop spectrophotometer (Quawell Q9000) by ultraviolet absorbance at 260 nm, and samples were stored at 4 °C.

K10-nkPEG Coating of DONs

DONs were mixed in a 3:1 (v/v) ratio with K10-1kPEG and K10-5kPEG solutions (Alamanda Polymers) at the required concentrations to obtain the desired 1:1 N/P coating ratio (nitrogens in amines/phosphates in DNA), as previously described,[15] and subsequently incubated overnight at room temperature. Uncoated DONs were equally diluted in Milli-Q prior to their use for comparison purposes.

Negative-Stain Transmission Electron Microscopy Imaging

CF400-Cu grids (Electron Microscopy Sciences) were subjected to a glow discharge treatment (30 s, 1 mA) before pipetting onto them 8 μL of the corresponding DON solution at 3 nM. After 90 s of incubation, the deposited solutions were carefully blotted from the grids with filter paper, and 1.5 μL of 2% uranyl acetate solution (in H_2O, w/v) was subsequently pipetted. Excess staining solution was immediately removed with filter paper, and the grids were left to air dry. Imaging was conducted using a Talos L120C TEM operated at 80×10^3 V.

Standard Protein Corona Adsorption and Isolation Methodology

Glycerol gradients for protein−DON complexes isolation were formed in a 1.5 mL microcentrifuge tube (Beckman Coulter) adapting previous protocols.[30] In brief, six equal volumes of glycerol-containing PBS1X solutions were carefully pipetted into the tubes to lay the distinct layers, starting with a 45% glycerol concentration at the bottom and having a 5% glycerol decrease per subsequent layer. The tubes were then incubated overnight at 4 °C to favor the continuity of the gradients. The following day, 30 nM initial DON solutions (or the equivalent solution without DON for the non-DON control) were mixed in a 1:3 (v/v) ratio with Dulbecco's modified Eagle's medium (DMEM) high glucose with L-glutamine and sodium pyruvate supplemented with 10% FBS (PAN-Biotech) in a total volume of 120 μL and subsequently incubated for 1 h under static conditions at 37 °C to allow for the stable formation of a protein corona. Six replicates per DON condition were incubated in parallel, including a no-DON condition as a control to avoid false positive results. Right after incubation, glycerol was added to the samples up to a final 15% (v/v) concentration and immediately loaded on top of a six-layer linear glycerol gradient (45 to 20% glycerol in PBS1X—Gibco), reaching a total volume of 1.2 mL. Once the samples were loaded on the gradients, they were subjected to a rate-zonal centrifugation process at 150,000 rcf at 4 °C for 120 min in an Optima MAX-XP Tabletop Ultracentrifuge (Beckman Coulter) to sediment and isolate the protein−DON complexes. The total volume of the tubes was then immediately fractionated in 10 equal volumes for downstream analysis of the process, and pellets were resuspended and retrieved in 120 μL of PBS1X solution. Cy5 fluorescence intensity and absorbance at 280 nm of each retrieved volume were eventually measured with a Cytation 5 imaging reader (BioTek) instrument to assess the yield of DON retrieval and effectiveness of protein isolation.

Sample Preparation and LC−MS Analysis

A total of six protein−DON pellet fractions were retrieved per DON coating condition and pooled in pairs for analysis. Samples were separated by SDS-PAGE on a 12% polyacrylamide gel and stained with Coomassie blue. Each gel lane was entirely sliced and subjected to in-gel digestion. The gel pieces were washed twice with 50% ethanol in 50 mM ammonium bicarbonate (AB, Sigma-Aldrich) for 20 min and dried by vacuum centrifugation. Proteins were reduced with 10 mM dithioerythritol (Merck-Millipore) for 1 h at 56 °C followed by a washing-drying step, as described above. Reduced proteins were alkylated with 55 mM iodoacetamide (Sigma-Aldrich) for 45 min at 37 °C in the dark followed by a washing-drying step, as described above. Proteins were digested overnight at 37 °C using mass spectrometry grade Trypsin gold (Trypsin Gold, Promega) at a concentration of 12.5 ng/μL in 50 mM AB supplemented with 10 mM $CaCl_2$. Resulting peptides were extracted in 70% ethanol, 5% formic acid (Merck-Millipore) twice for 20 min, dried by vacuum centrifugation. Resulting peptides were desalted on StageTips[31] and dried under a vacuum concentrator. For liquid chromatography and mass spectrometry (LC−MS)/MS analysis, resuspended peptides were separated by reversed phase chromatography on a Dionex Ultimate 3000 RSLC nano UPLC system in-line connected to an Exploris 480 Orbitrap mass spectrometer (Thermo Fisher Scientific).

Label-Free Data Analysis

Raw data were processed using MaxQuant[32] (version 1.6.10.43) and searched against a database consisting of the Bos Taurus Reference proteome database (37,513 protein sequences Release2021_02). Carbamidomethylation was set as fixed modification, whereas oxidation (M), phosphorylation (S, T, and Y), acetylation (Protein N-term), and glutamine to pyroglutamate were considered as variable modifications. A maximum of two missed cleavages were allowed, and a "Match between runs" option was enabled. A minimum of two peptides was

https://doi.org/10.1021/acspolymersau.3c00009
ACS Polym. Au 2023, 3, 344−353

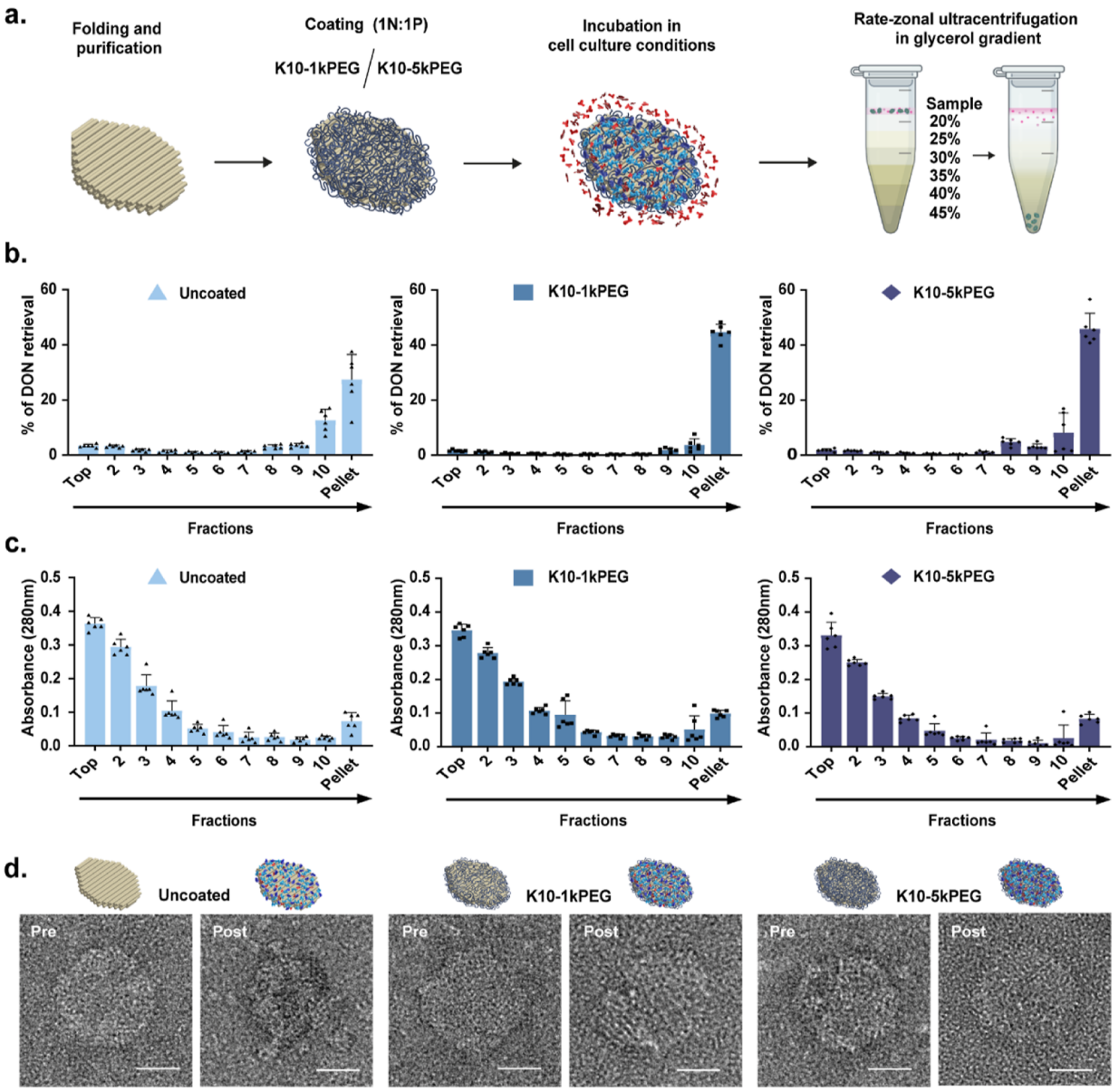

Figure 1. Formation and isolation of protein corona−DON complexes. (a) Schematic overview of the methodology to enable protein corona formation and isolate protein−DNA complexes from unbound proteins. (b) Percentage (%) of DON retrieval for each of the fractionated volumes based on the corresponding Cy5 fluorescence intensity measured. Percentages are relative to the original DON concentration. Data are represented as mean ± SD, $n = 6$. (c) Profile of the protein content in the gradient based on absorbance measurements at 280 nm. Data are represented as mean ± SD, $n = 6$ in one independent experiment. (d) TEM images of non-treated DONs (Pre) and DONs incubated in proteins and retrieved via rate-zonal centrifugation (Post). Scale bars are 25 nm.

required for protein identification, and the false discovery rate cutoff was set to 0.01 for both peptides and proteins. Label-free quantification (LFQ) and normalization were performed by MaxQuant using the MaxLFQ algorithm, with the standard settings.[33] The statistical analyses of the label-free data were performed using Perseus[34] (version 1.6.15.0) from the MaxQuant tool suite. Reverse proteins, potential contaminants, and proteins only identified by sites were filtered out. Protein groups containing at least three valid values in at least one group were conserved for further analysis. Empty values were imputed with random numbers from a normal distribution (width: 0.3 and down shift: 1.8). A two-sample t test was performed to determine significant differentially abundant candidates. Proteins were considered significant when they had a $p < 0.05$. Relative protein abundance (RPA) was calculated by averaging the protein peak intensity-based absolute quantification (iBAQ) values of the replicates and deducting the corresponding no-DON control values. Protein molecular weights and isoelectric points were calculated with the Compute pI/MW tool on the ExPASy Server. Protein Venn diagrams and heatmaps were plotted using R.

Single-Protein Corona Pre-formation

We computed the number of proteins that would be adsorbed on our hexagonal DONs assuming the formation of a perfect monolayer with a hexagonal lattice and considering bovine serum albumin (BSA) as an average protein model. For corona pre-formation, DONs were incubated in a volume containing a six-fold larger amount of proteins than the estimated number. More precisely, DONs (uncoated, K10-1kPEG or K10-5kPEG, initially concentrated at 30 nM) were mixed with murine protein stock solutions (ApoH: #784906, BioLegend, hemoglobin: #CSB-NP004901m, Cusabio, or clusterin: #50485-M08H, Sino Biological, initially at 0.5 mg/mL in PBS1X; also BSA: #A2153, Sigma-Aldrich, for Supporting Information) in a final volume containing 5 nM DONs, 0.3 mg/mL protein, and a restored 10 mM

https://doi.org/10.1021/acspolymersau.3c00009
ACS Polym. Au 2023, 3, 344−353

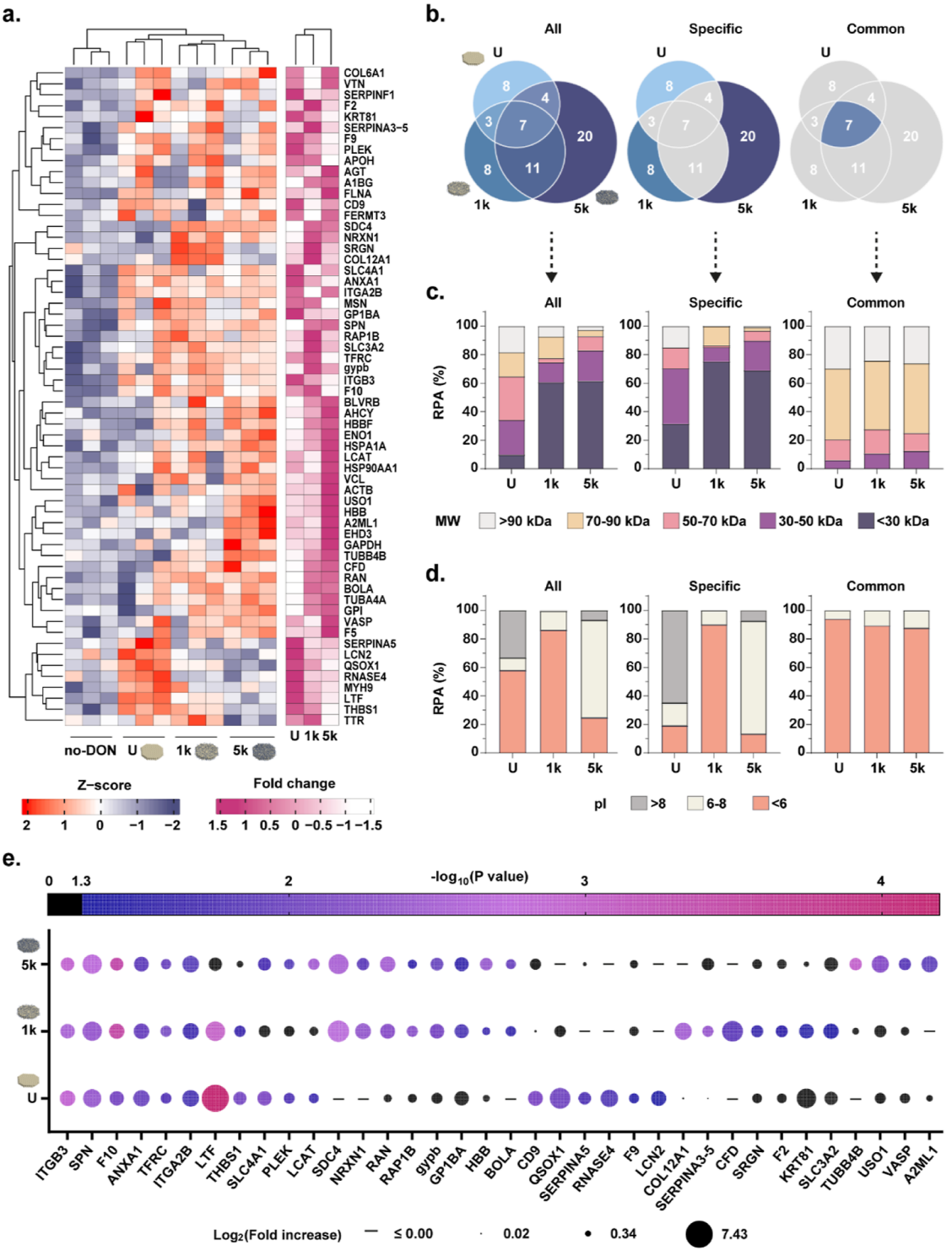

Figure 2. Characterization of protein corona composition of uncoated (U), K10-1kPEG (1k), and K10-5kPEG (5k) DONs. (a) Clustered heat map based on LFQ intensities displaying *Z*-score and fold change with respect the no-DON control of all characterized significantly adsorbed proteins. *Z*-score represents the distance of the corresponding LFQ intensity value, in standard deviations, from the mean of each protein. Each row is scaled separately across all samples. Black = non-significant adsorption (*p*-value > 0.05). (b) Venn diagram of adsorbed proteins (*p*-value ≤0.05) onto each DON type, highlighting subgroups (all, specific, and common) considered for respective analysis in (c,d). (c) RPA based on iBAQ values of the distinct proteins significantly adsorbed in function of their molecular weight (MW). (d) RPA of the distinct characterized proteins significantly adsorbed in function of their isoelectric point (pI). (e) Bubble plot displaying fold increase and significance degree of those proteins adsorbed with a *p*-value ≤0.05 and a minimum two-fold enrichment for at least one of the DON conditions.

$MgCl_2$ final concentration through the addition of $MgCl_2$-containing PBS1X to ensure the integrity of uncoated DONs. The total mixed volume was then incubated at 37 °C for 1 h under static conditions to allow for stable protein adsorption.

https://doi.org/10.1021/acspolymersau.3c00009
ACS Polym. Au 2023, 3, 344−353

Cellular Uptake Study by Flow Cytometry

RAW 264.7 MF cells (35×10^3) were seeded overnight in 96-well flat bottom plates (Corning) at 37 °C with 5% CO_2. Incubation of uncoated, K10-1kPEG, or K10-5kPEG DONs for single-protein corona pre-formation was carried out in a total volume of 10 μL for the distinct protein conditions, as well as in 10% FBS as representative of the standard protein adsorption that would take place in cell medium. Afterward, the medium from the cells was removed, and 50 μL of DONs diluted in 10% FBS-containing RAW medium was added at the final DON concentration of 1 nM and incubated for 2 h at 37 °C. To digest all non-internalized DONs,[15] medium was removed, and cells were incubated for 1 h at 37 °C in 50 μL of DNAse I in RAW medium (70 U/mL, Sigma-Aldrich). Next, cells were detached, resuspended in PBS1X, and transferred to V-bottom plates. RAW 264.7 MF cells were stained with live/dead fixable yellow dead cell stain in PBS1X (L34967, Thermo Fisher Scientific) and resuspended in FACS BSA stain buffer (BD Biosciences). Cells were acquired on a LSR Fortessa analyzer (BD Biosciences) using FACSDiva software. Data were analyzed using FlowJo software (version 10.0.7r2), and RAW 254.7 MF cells were gated on single cells and live/dead fixable yellow-negative cells.

Cellular Uptake Study by Confocal Microscopy

RAW 264.7 MF cells (10×10^3) were seeded overnight in 12-well slides (ibidi) at 37 °C with 5% CO_2. K10-1kPEG and K10-5kPEG DONs were incubated for protein corona pre-formation, as described above for uptake studies by flow cytometry. After 1 h incubation of DONs, the medium from the cells was removed, 70 μL of DONs diluted in 10% FBS-containing RAW medium was added at a final DON concentration of 1 nM and incubated for 2 h at 37 °C. To digest non-internalized DONs, medium was removed immediately after, and cells were incubated for 1 h at 37 °C with 70 μL of DNAse I (70 U/mL).[15] Next, cells were washed with PBS1X and fixed by incubating them at room temperature for 8 min with 100 μL of 4% paraformaldehyde (PFA). Cells were subsequently thoroughly washed with PBS1X and stained with 70 μL of DAPI solution (300 nM, Thermo Fisher) at room temperature for 4 min. After washing out, all the solutions were pipetted out from the wells, removing the plastic wells and leaving the glass to air dry at room temperature for 15 min. ProLong glass antifade mountant (Invitrogen) was then deposited on the slide, which was covered right afterward with a coverslip and left to air-dry at room temperature for 24 h. Sample imaging was conducted on a Leica TCS SP8 confocal microscope with a HC PL APO 63×/1.40 OIL CS2 (Leica) objective. For DAPI and Cy5 signals, 405 and 639 nm wavelength excitation lasers and 415/55 and 650/50 filters were used, respectively (DAPI for K10-1kPEG and K10-5kPEG DONs: 10% intensity, 100% gain; Cy5 for K10-1kPEG: 1% intensity, 50% gain; Cy5 for K10-5kPEG: 2% intensity, 50% gain). Images were acquired with a Leica DFC7000 GT camera, and image analysis was performed with ImageJ software (version 1.53t) through manual cell segmentation.

RESULTS AND DISCUSSION

As a central DON subject for this study, we employed a multilayer, disk-shaped object (Figure 1a), extensively characterized in previous work and compliant with the design parameters specified for the cell uptake.[29,35,36] This rigid, solid disk is 60 nm in diameter and 7 nm thick and carries six integrated Cy5 dyes. These DONs were coated with an oligolysine-PEG diblock co-polymer in a 1:1 N/P ratio (nitrogen in lysine to phosphorous in DNA) with peptides of 10 L-lysine monomers (K10) conjugated to PEG blocks of either 1 kDa (1kPEG) or 5 kDa (5kPEG). While the positively charged lysine residues bind electrostatically to the DNA backbone and stabilize the intrinsic repulsive forces of DNA nanoparticles, the PEG block restrains nuclease action and particle aggregation by steric hindrance. Importantly, this coating ensures a long-lasting protection of the DONs without altering their shape nor hindering their cellular internalization, and it is expected to neutralize the original negative surface charge of DNA structures when applied in a 1:1 N/P ratio.[15] Proper folding, purification, and coating of the structures were verified by agarose gel electrophoresis (AGE) (Figure S1). To allow for adsorption of a stable protein corona representative of standard cell culture conditions, uncoated, K10-1kPEG-, and K10-5kPEG-coated DONs were each incubated in at 37 °C in DMEM medium supplemented with 10% FBS for 1 h.

To enable the proteomic profiling of the coronae adsorbed onto DONs, it was imperative to separate the protein−DNA complexes from unbound proteins. Due to the similarities in size and density between DNA and proteins, current DON corona studies have been restricted to magnetic-based separation,[13] whose effectiveness requires the introduction of design modifications that might bias protein adsorption.[37] Here, we chose to isolate the protein−DNA complexes with a one-step rate-zonal centrifugation process involving the use of a glycerol density gradient. This technique has proven to be effective for post-folding purification of DONs[30] and is entirely label free, though potentially disturbing the more loosely bound proteins of the soft corona to a higher extent. Following corona formation, solutions were loaded on top of a six-layer glycerol gradient (20−45%) (Figure 1a). A no-DON control consisting of only the protein-containing medium was included to account for false positive results due to sedimentation of protein aggregates. Immediately after centrifugation, the total volume of the solution was fractionated and the pellets resuspended and retrieved. The DON and protein contents of each fraction were subsequently analyzed through fluorescence and absorbance measurements, respectively, and pelleted DON integrity was examined by transmission electron microscopy (TEM).

For all DONs (uncoated, K10-1kPEG, and K10-5kPEG-coated), most of the nanoparticles could be retrieved from the resuspended pellet (Figure 1b). The reduced retrieval of the uncoated DONs can be explained by the instability of these unprotected structures when facing nuclease action and low salt concentrations, as supported by TEM (Figure S2). Profiling of the protein content per fraction through absorbance measurements at 280 nm revealed a clear decreasing trend in protein concentration toward higher glycerol zones (Figure 1c). In comparison to the no-DON control, we observed an apparent increase in the 280 nm absorbance in the resuspended pellet which contains most of the DONs (Figure S3). This signal increase is a combined effect of the DNA particles content and their protein corona, as subsequently examined by the proteomic analysis. Next, we visualized the structural integrity of all conditions with TEM (Figures 1d and S2). The presence of partially disintegrated structures in the uncoated samples indeed confirms that their stability was compromised. On the contrary, K10-1kPEG and K10-5kPEG DONs displayed similar morphologies to their non-treated counterparts, proving efficient protection and structural integrity during the established workflow.

Effect of Polymer Coatings on Protein Corona Compositions

Following isolation of the protein−DNA complexes, we characterized the corona composition via a LFQ proteomic strategy after separation through LC−MS (Figure 2 and Table S1). A larger number of protein species was identified for all DON-containing samples in comparison to the no-DON control, confirming the presence of a protein corona (Figure S4). Proteins significantly adsorbed on at least one of the DON conditions were plotted in heatmaps ranked by their Z-score and

https://doi.org/10.1021/acspolymersau.3c00009
ACS Polym. Au 2023, 3, 344−353

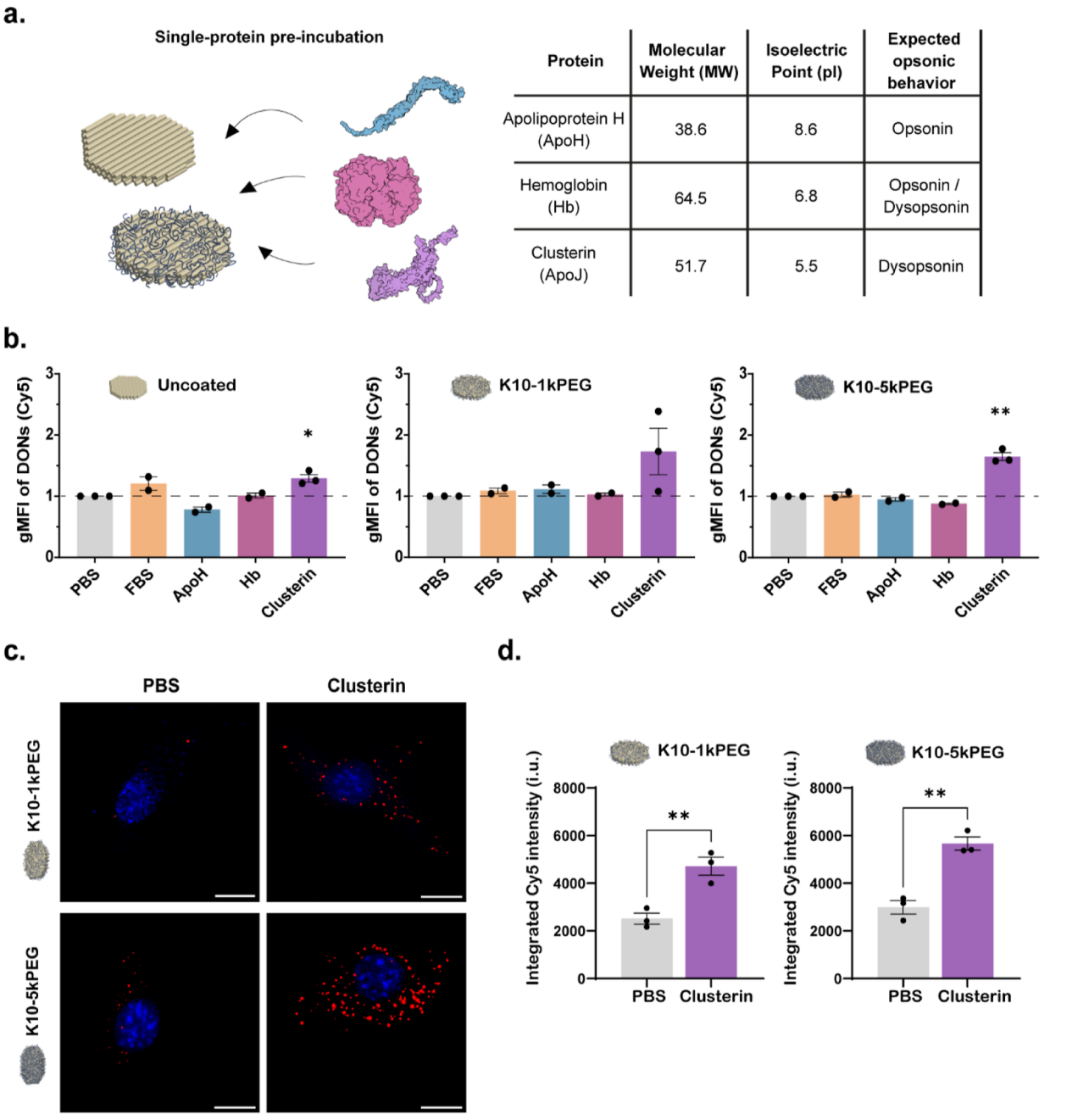

Protein	Molecular Weight (MW)	Isoelectric Point (pI)	Expected opsonic behavior
Apolipoprotein H (ApoH)	38.6	8.6	Opsonin
Hemoglobin (Hb)	64.5	6.8	Opsonin / Dysopsonin
Clusterin (ApoJ)	51.7	5.5	Dysopsonin

Figure 3. Impact of protein corona customization on DON cell internalization. (a) Schematic overview and characteristics of the proteins selected for engineering the protein corona around our uncoated and coated DONs through a single protein pre-incubation step. (b) Quantification through flow cytometric analysis of the uptake of 1 nM uncoated, K10-1kPEGK, and K10-5kPEG DONs after 120 min by RAW 264.7 macrophages expressed as geometric mean fluorescence intensity of Cy5 relative to PBS. Data are represented as mean ± SEM, n = 2 or 3 in two or three independent experiments. Statistical significance was determined with a one-sample t test on log-transformed data. *$p \leq 0.0330$ and **$p \leq 0.0057$. (c,d) Uptake of 1 nM K10-1kPEGK and K10-5kPEG DONs after 120 min by RAW 264.7 macrophages after clusterin corona pre-formation. (c) Representative confocal microscopy images of the assay. Nuclei stained with DAPI (blue), DON Cy5 in red. Scale bars are 10 μm. (d) Quantification of uptake through analysis of confocal images expressed as integrated Cy5 intensity. i.u.: intensity units. Data are represented as mean ± SEM, n = 3 in three independent experiments. Statistical significance was determined with a t test. **$p \leq 0.008$ for K10-1kPEGK DONs and **$p \leq 0.002$ for K10-5kPEGK DONs.

fold increase with respect to the no-DON control (Figure 2a). Remarkably, none of the PEG polymer coatings reduced the diversity of proteins adsorbing onto the DONs, though significantly altered each adsorption profile (Figure 2b): while certain proteins were present in the corona of all DON conditions ("common proteins"), many others were adsorbed in only one ("specific proteins") or two of the polymer coatings.

To better understand the relation between the type of polymeric coating and the nature of the adsorbed proteins, we focused on the physical characteristics of the identified proteins. The relative abundance of significantly adsorbed proteins in each DON coating condition was calculated through a peak iBAQ analysis. The corona of uncoated DONs predominately consists of high-molecular-weight (MW) proteins, that is larger than 50 kDa, while smaller proteins were prevalent for both

https://doi.org/10.1021/acspolymersau.3c00009
ACS Polym. Au 2023, 3, 344−353

K10PEG-coated conditions (Figure 2c). Interestingly, most of the "common proteins" were larger than 70 kDa. Indeed, previous PEGylation studies with 5 kDa chains reported the need of grafting densities larger to the 0.25 PEG/nm^2 of our coating conditions to attain a drastic decrease in unspecific protein adsorption.[38] At our grafting densities, the K10-1kPEG (Flory radius R = 2.25 nm) coating is expected to have an intermediate brush conformation (mushroom-brush), while the longer polymeric chains of the K10-5kPEG (R = 6 nm) coating present a thicker, defined brush.[39] Steric repulsion in the coated conditions is enough to hinder the interaction with large molecules while yet allowing and favoring the intercalation and residence of small proteins between the PEG chains.

In depth analysis of the isoelectric points revealed that electrostatic interactions are a major driving force of the corona formation for DONs (Figure 2d). In particular, the corona of uncoated DONs was mostly composed of negatively charged proteins, though still containing a substantial fraction (∼35%) of positive proteins. In contrast, almost 90% of the corona content for K10-1kPEG DONs was negatively charged proteins, whereas near-neutral proteins accounted for over 70% of the proteins adsorbed on K10-5kPEG DONs. The distinct affinity of each differentially coated DON toward proteins of a certain charge is further confirmed by the predominant isoelectric point values among the respective "specific proteins". Nevertheless, close to 90% of the "common proteins" were like DNA-negatively charged, suggesting cation mediated-electrostatic bridging.[40] The longer 5 kDa PEG chains seem to successfully shield the surface, while the thinner and irregular K10-1kPEG coating might not avoid the exposure of positive lysine residues, encouraging the adsorption of negatively charged proteins.

For a comprehensive picture of the individual protein contributions to the distinct adsorption profiles, we determined the most enriched proteins in DONs (uncoated, K10-1kPEG, and K10-5kPEG) and displayed their fold increase with respect to a no-DON control (Figure 2e). Out of the "common proteins" identified, sialophorin (SPN or CD43) and annexin A1(ANXA1) proteins are substantially enriched. The SPN protein has been reported to induce the DNA-binding activity of certain transcription factors.[41] More interestingly, ANXA1 presents DNA helicase activity, binding double-stranded DNA in the presence of Mg^{2+}.[42] Among proteins preferentially adsorbed on uncoated DONs, lactoferrin stands out, confirming previous DNA nanoparticle corona studies.[13] This glycoprotein has two DNA-binding sites that allow the molecule to interact specifically and non-specifically with single- and double-stranded DNA,[43] presenting Mg^{2+}-dependent DNase activity while also acting as a transcription factor.[44,45] Quiescin sulfhydryl oxidase 1, involved in DNA damage responses, also favors the uncoated DON corona.[46]

Inversely, a series of proteins are predominantly found in the PEGylated DON coronae, most noticeably the small (21.6 kDa) syndecan-4, a proteoglycan receptor controlling multiple endocytic pathways.[47] The metalloprotein hemoglobin subunit β (HBB, 16 kDa), previously reported to interact with DNA nanostructures, increases abundance in PEGylated DONs following literature that correlates HBB adsorption to PEG length.[48] This observation also follows our previous finding that the bulkier coatings (e.g., K10-5kPEG) favor adsorption of smaller proteins. Both PEG coatings encouraged the adsorption of different specific proteins, with complement factor D present in K10-1kPEG-coated DONs and alpha-2 macroglobulin-like 1 (A2ML1) enriched for K10-5kPEG coatings. Both proteins are part of the complement system, which mediates opsonization.[49] Interestingly, none of the conditions demonstrated significant adsorption levels of BSA, despite BSA being a majoritarian protein in the serum of origin and the corona of previously studied DONs.[13] A BSA-DON interaction test confirmed that BSA binding—if existing at all—is very weak, hence likely present in the easily disturbed soft corona (Figure S5).

Manipulation of Coronae to Bias the Cellular Uptake

Due to the prominent role, the protein corona plays at the material−cell interface, manipulating the corona could provide an engineering strategy to control cellular internalization of matter. As the corona of a particle incubated in biological media preserves a fingerprint of that specific environment,[50] a single-protein pre-incubation solution can serve to enrich the corona for a molecule of interest and bias its final equilibrium composition.[28,51,52] To manipulate cell internalization of DONs through biased corona formation, we selected three proteins varying in surface charge and expected opsonic (uptake enhancing) behaviors (Figures 3a and S6). Murine apolipoprotein H (apoH) is a positively charged protein at physiological conditions, found to be present in the corona of the uncoated DONs and other PEGylated nanoparticles, and known to promote the phagocytic uptake.[27] Clusterin (ApoJ), a negatively charged protein, has expected dysopsonin (uptake inhibiting) behavior since its presence in the corona of PEGylated nanoparticles is amply reported to contribute to the stealth effect.[17] Murine hemoglobin (Hb), a near-neutrally charged protein and present in coated DONs, has ambiguous opsonic behavior.[48]

The interaction between the selected proteins and our pre-incubated nanoparticles was analyzed and confirmed through electrophoretic mobility shift assays after fixation of the corona with PFA to prevent disruption by the applied electric field (Figure S7). A dose−response analysis determined that level of protein−DNA interaction reflected by a change in electrophoretic mobility correlates well with the amount of protein (Figure S8). In addition, we verified that corona pre-formation did not have a major influence neither on the long-term stability of the uncoated DONs nor on the protective capacity of the coatings following a 24 h-long incubation of the pre-incubated DONs in standard cell culture conditions (Figure S9).

To investigate the effect on cellular internalization, we presented the protein pre-treated (ApoH, Hb, clusterin, or 10% FBS control) DONs to murine RAW 264.7 macrophage cells (MF), previously reported to efficiently take up these DONs.[29] Culture medium was refreshed after 2 h of incubation, when the peak uptake of DONs was reached (Figure S10). To digest any extracellular membrane-bound DON, cells were exposed to high concentrations of DNAse I,[29,36] and the uptake was quantified through flow cytometric analysis. All cells showed excellent viability, and differential uptake in function of the coating state of the DONs was observed, with a preferential uptake for the K10-1kPEG-coated material (Figure S11). The majority of pre-treated DONs showed a highly comparable uptake profile; however, the pre-adsorption of clusterin on polymer-coated DONs led to a significant enhancement of the uptake (Figures 3b and S12). This observation contrasts the reported influence of clusterin on the stealth effect of PEGylated particles, classifying this protein with dysopsonin function, yet several other studies have indeed noticed the opsonic nature, connected to its role in clearance of apoptotic cells and cellular debris by interaction with endocytic receptors.[53,54] It is thus

https://doi.org/10.1021/acspolymersau.3c00009
ACS Polym. Au 2023, 3, 344−353

possible that the DNA-oligolysine-PEG system favors the opsonic functionality of the clusterin when adsorbed onto it. However, given the dynamic nature of the protein corona, we speculate that the pre-complexation of clusterin might promote the preferential adsorption of alternative proteins from the medium (e.g., opsonins), leading to the formation of a new, biased corona whose overall influence encourages the opsonization of the stabilized DONs. This overruling mechanism of the clusterin stealth effect has also been proposed for other stealth polymers.[55]

Finally, the increase in the uptake after the pre-adsorption of a clusterin corona on coated DONs was confirmed through a quantitative fluorescence analysis following confocal microscopy. Visual qualitative inspection of the confocal images showed the classic punctate fluorescence signature, known to result from endo-lysosomal entrapped DONs (Figure 3c). Quantification of the integral fluorescence intensity indeed confirmed the preferential cellular uptake of clusterin pretreated DONs for polymer-stabilized conditions (Figure 3d). Overall, these results confirm the possibility to bias the endocytosis of oligolysine-PEG-stabilized DONs by the preformation of a protein corona through a simple protein−DNA co-incubation process.

CONCLUSIONS

We have assessed the impact of the DON-stabilizing oligolysine-PEG coating on protein adsorption and explored the possibility to influence the cellular uptake of stabilized DONs by intentionally biasing corona formation through custom protein pre-incubation. For studying the protein corona adsorbed around polymerically stabilized DONs without the need of structural modifications, we leveraged an accessible isolation methodology based on rate-zonal centrifugation. The identification and quantification of the different protein coronae around DONs when submerged in cell culture conditions indicate that oligolysine-PEG polymer coatings indeed modulate protein adsorption. They effectively modify the particle's surface charge and chemical composition as well as present a physical steric barrier restricting larger molecules to interact. As such, PEG coatings favor the adsorption of smaller proteins that are negatively or near-neutrally charged. Finally, we demonstrated that the pre-formation of a clusterin corona on stabilized DONs significantly enhances the macrophage uptake, paving the way for future in-depth evaluations and customized applications of this simple engineering approach. Overall, our results advance the fundamental understanding on molecular interface changes resulting from the application of oligolysine-PEG as a stabilizing strategy in bioengineering applications of DONs and provide an accessible strategy to influence their cellular uptake.

ASSOCIATED CONTENT

Supporting Information

The Supporting Information is available free of charge at https://pubs.acs.org/doi/10.1021/acspolymersau.3c00009.

AGE, PAGE, protein−DON interaction tests, stability assays, cell culture and statistical analysis methodology; data availability; DON characterization AGE; TEM of isolated DONs; no-DON centrifugation profiles; number of identified proteins; protein interaction test (AGE); SDS-PAGE of selected proteins; stability assays; uptake kinetics; impact of coatings on uptake; flow cytometric gating, percentage of live and positive cells and flow cytometric histograms; and proteomic results (PDF)

List of proteins identified by LC-MS that adsorb significantly onto DONs (XLSX)

AUTHOR INFORMATION

Corresponding Author

Maartje M. C. Bastings − *Programmable Biomaterials Laboratory, Institute of Materials, Interfaculty Bioengineering Institute, School of Engineering, Ecole Polytechnique Fédérale Lausanne, Lausanne 1015, Switzerland;* orcid.org/0000-0002-7603-4018; Email: maartje.bastings@epfl.ch

Authors

Hugo J. Rodríguez-Franco − *Programmable Biomaterials Laboratory, Institute of Materials, Interfaculty Bioengineering Institute, School of Engineering, Ecole Polytechnique Fédérale Lausanne, Lausanne 1015, Switzerland;* orcid.org/0009-0008-7819-1624

Jorieke Weiden − *Programmable Biomaterials Laboratory, Institute of Materials, Interfaculty Bioengineering Institute, School of Engineering, Ecole Polytechnique Fédérale Lausanne, Lausanne 1015, Switzerland;* orcid.org/0000-0002-2485-0590

Complete contact information is available at: https://pubs.acs.org/10.1021/acspolymersau.3c00009

Author Contributions

CRediT: **Hugo José Rodriguez-Franco** data curation (lead), formal analysis (lead), investigation (lead), methodology (lead), visualization (lead), writing-original draft (lead); **Jorieke Weiden** data curation (supporting), formal analysis (supporting), methodology (supporting), validation (supporting); **Maartje M.C. Bastings** conceptualization (lead), funding acquisition (lead), methodology (supporting), project administration (lead), supervision (lead), validation (lead), writing-review & editing (lead).

Notes

The authors declare no competing financial interest.

ACKNOWLEDGMENTS

This work was funded by the European Research Council (ERC) Horizon 2020 Excellent Science program (grant 948334 InActioN). The authors like to thank the support of the EPFL Proteomics Core Facility, especially Romain Hamelin and Florence Armand, for proteomics sample preparation and LC−MS processing. We are grateful to the EPFL Interdisciplinary Centre for Electron Microscopy (CIME), especially Davide Demurtas for training and guidance in instrument operation, the EPFL Bioimaging and Optics Platform (BIOP) for insightful discussion and instrument training. The authors thank Dr. Guido van Mierlo for guidance in proteomic analysis and Vincenzo Caroprese and Kaltrina Paloja for insightful discussions and guidance on image analysis.

REFERENCES

(1) Tenzer, S.; Docter, D.; Kuharev, J.; Musyanovych, A.; Fetz, V.; Hecht, R.; Schlenk, F.; Fischer, D.; Kiouptsi, K.; Reinhardt, C.; Landfester, K.; Schild, H.; Maskos, M.; Knauer, S. K.; Stauber, R. H. Rapid Formation of Plasma Protein Corona Critically Affects Nanoparticle Pathophysiology. *Nat. Nanotechnol.* **2013**, *8*, 772−781.

(2) Hajipour, M. J.; Safavi-Sohi, R.; Sharifi, S.; Mahmoud, N.; Ashkarran, A. A.; Voke, E.; Serpooshan, V.; Ramezankhani, M.; Milani, A. S.; Landry, M. P.; Mahmoudi, M. An Overview of Nanoparticle Protein Corona Literature. *Small* **2023**, 2301838.
(3) García-Álvarez, R.; Vallet-Regí, M. Hard and Soft Protein Corona of Nanomaterials: Analysis and Relevance. *Nanomaterials* **2021**, *11*, 888.
(4) Barbero, F.; Russo, L.; Vitali, M.; Piella, J.; Salvo, I.; Borrajo, M. L.; Busquets-Fité, M.; Grandori, R.; Bastús, N. G.; Casals, E.; Puntes, V. Formation of the Protein Corona: The Interface between Nanoparticles and the Immune System. *Semin. Immunol.* **2017**, *34*, 52−60.
(5) Zhang, Y.; Wu, J. L. Y.; Lazarovits, J.; Chan, W. C. W. An Analysis of the Binding Function and Structural Organization of the Protein Corona. *J. Am. Chem. Soc.* **2020**, *142*, 8827−8836.
(6) Li, X.; He, E.; Jiang, K.; Peijnenburg, W. J. G. M.; Qiu, H. The Crucial Role of a Protein Corona in Determining the Aggregation Kinetics and Colloidal Stability of Polystyrene Nanoplastics. *Water Res.* **2021**, *190*, 116742.
(7) Corbo, C.; Molinaro, R.; Parodi, A.; Toledano Furman, N. E.; Salvatore, F.; Tasciotti, E. The Impact of Nanoparticle Protein Corona on Cytotoxicity, Immunotoxicity and Target Drug Delivery. *Nanomedicine* **2016**, *11*, 81−100.
(8) Fleischer, C. C.; Payne, C. K. Nanoparticle−Cell Interactions: Molecular Structure of the Protein Corona and Cellular Outcomes. *Acc. Chem. Res.* **2014**, *47*, 2651−2659.
(9) Wang, P.; Meyer, T. A.; Pan, V.; Dutta, P. K.; Ke, Y. The Beauty and Utility of DNA Origami. *Chem* **2017**, *2*, 359−382.
(10) Chinen, A. B.; Guan, C. M.; Ko, C. H.; Mirkin, C. A. The Impact of Protein Corona Formation on the Macrophage Cellular Uptake and Biodistribution of Spherical Nucleic Acids. *Small* **2017**, *13*, 1603847.
(11) Chinen, A. B.; Guan, C. M.; Mirkin, C. A. Spherical Nucleic Acid Nanoparticle Conjugates Enhance G-Quadruplex Formation and Increase Serum Protein Interactions. *Angew. Chem., Int. Ed. Engl.* **2015**, *127*, 537−541.
(12) Lorents, A.; Maloverjan, M.; Padari, K.; Pooga, M. Internalisation and Biological Activity of Nucleic Acids Delivering Cell-Penetrating Peptide Nanoparticles Is Controlled by the Biomolecular Corona. *Pharmaceuticals* **2021**, *14*, 667.
(13) Xu, F.; Dong, B.; Li, X.; Gao, F.; Yang, D.; Xue, W.; Wang, P. Profiling and Regulating Proteins That Adsorb to DNA Materials in Human Serum. *Anal. Chem.* **2021**, *93*, 8671−8679.
(14) Hahn, J.; Wickham, S. F. J.; Shih, W. M.; Perrault, S. D. Addressing the Instability of DNA Nanostructures in Tissue Culture. *ACS Nano* **2014**, *8*, 8765−8775.
(15) Ponnuswamy, N.; Bastings, M. M. C.; Nathwani, B.; Ryu, J. H.; Chou, L. Y. T.; Vinther, M.; Li, W. A.; Anastassacos, F. M.; Mooney, D. J.; Shih, W. M. Oligolysine-Based Coating Protects DNA Nanostructures from Low-Salt Denaturation and Nuclease Degradation. *Nat. Commun.* **2017**, *8*, 15654.
(16) Shi, L.; Zhang, J.; Zhao, M.; Tang, S.; Cheng, X.; Zhang, W.; Li, W.; Liu, X.; Peng, H.; Wang, Q. Effects of Polyethylene Glycol on the Surface of Nanoparticles for Targeted Drug Delivery. *Nanoscale* **2021**, *13*, 10748−10764.
(17) Schöttler, S.; Becker, G.; Winzen, S.; Steinbach, T.; Mohr, K.; Landfester, K.; Mailänder, V.; Wurm, F. R. Protein Adsorption Is Required for Stealth Effect of Poly(Ethylene Glycol)- and Poly-(Phosphoester)-Coated Nanocarriers. *Nat. Nanotechnol.* **2016**, *11*, 372−377.
(18) Zagorovsky, K.; Chou, L. Y. T.; Chan, W. C. W. Controlling DNA−Nanoparticle Serum Interactions. *Proc. Natl. Acad. Sci. U.S.A.* **2016**, *113*, 13600−13605.
(19) Lacroix, A.; Edwardson, T. G. W.; Hancock, M. A.; Dore, M. D.; Sleiman, H. F. Development of DNA Nanostructures for High-Affinity Binding to Human Serum Albumin. *J. Am. Chem. Soc.* **2017**, *139*, 7355−7362.
(20) Estrich, N. A.; Hernandez-Garcia, A.; de Vries, R.; LaBean, T. H. Engineered Diblock Polypeptides Improve DNA and Gold Solubility during Molecular Assembly. *ACS Nano* **2017**, *11*, 831−842.
(21) Auvinen, H.; Zhang, H.; Nonappa; Kopilow, A.; Niemelä, E. H.; Nummelin, S.; Correia, A.; Santos, H. A.; Linko, V.; Kostiainen, M. A. Protein Coating of DNA Nanostructures for Enhanced Stability and Immunocompatibility. *Adv. Healthcare Mater.* **2017**, *6*, 1700692.
(22) Xu, X.; Fang, S.; Zhuang, Y.; Wu, S.; Pan, Q.; Li, L.; Wang, X.; Sun, X.; Liu, B.; Wu, Y. Cationic Albumin Encapsulated DNA Origami for Enhanced Cellular Transfection and Stability. *Materials* **2019**, *12*, 949.
(23) Mikkilä, J.; Eskelinen, A.-P.; Niemelä, E. H.; Linko, V.; Frilander, M. J.; Törmä, P.; Kostiainen, M. A. Virus-Encapsulated DNA Origami Nanostructures for Cellular Delivery. *Nano Lett.* **2014**, *14*, 2196−2200.
(24) Kopatz, I.; Zalk, R.; Levi-Kalisman, Y.; Zlotkin-Rivkin, E.; Frank, G. A.; Kler, S. Packaging of DNA Origami in Viral Capsids. *Nanoscale* **2019**, *11*, 10160−10166.
(25) Seitz, I.; Ijäs, H.; Linko, V.; Kostiainen, M. A. Optically Responsive Protein Coating of DNA Origami for Triggered Antigen Targeting. *ACS Appl. Mater. Interfaces* **2022**, *14*, 38515−38524.
(26) Mirshafiee, V.; Kim, R.; Park, S.; Mahmoudi, M.; Kraft, M. L. Impact of Protein Pre-Coating on the Protein Corona Composition and Nanoparticle Cellular Uptake. *Biomaterials* **2016**, *75*, 295−304.
(27) Ritz, S.; Schöttler, S.; Kotman, N.; Baier, G.; Musyanovych, A.; Kuharev, J.; Landfester, K.; Schild, H.; Jahn, O.; Tenzer, S.; Mailänder, V. Protein Corona of Nanoparticles: Distinct Proteins Regulate the Cellular Uptake. *Biomacromolecules* **2015**, *16*, 1311−1321.
(28) Simon, J.; Müller, L. K.; Kokkinopoulou, M.; Lieberwirth, I.; Morsbach, S.; Landfester, K.; Mailänder, V. Exploiting the Biomolecular Corona: Pre-Coating of Nanoparticles Enables Controlled Cellular Interactions. *Nanoscale* **2018**, *10*, 10731−10739.
(29) Koga, M. M.; Comberlato, A.; Rodríguez-Franco, H. J.; Bastings, M. M. C. Strategic Insights into Engineering Parameters Affecting Cell Type-Specific Uptake of DNA-Based Nanomaterials. *Biomacromolecules* **2022**, *23*, 2586−2594.
(30) Lin, C.; Perrault, S. D.; Kwak, M.; Graf, F.; Shih, W. M. Purification of DNA-Origami Nanostructures by Rate-Zonal Centrifugation. *Nucleic Acids Res.* **2013**, *41*, No. e40.
(31) Rappsilber, J.; Mann, M.; Ishihama, Y. Protocol for Micro-Purification, Enrichment, Pre-Fractionation and Storage of Peptides for Proteomics Using StageTips. *Nat. Protoc.* **2007**, *2*, 1896−1906.
(32) Cox, J.; Mann, M. MaxQuant Enables High Peptide Identification Rates, Individualized p.p.b.-Range Mass Accuracies and Proteome-Wide Protein Quantification. *Nat. Biotechnol.* **2008**, *26*, 1367−1372.
(33) Cox, J.; Hein, M. Y.; Luber, C. A.; Paron, I.; Nagaraj, N.; Mann, M. Accurate Proteome-Wide Label-Free Quantification by Delayed Normalization and Maximal Peptide Ratio Extraction, Termed MaxLFQ. *Mol. Cell. Proteomics* **2014**, *13*, 2513−2526.
(34) Tyanova, S.; Temu, T.; Sinitcyn, P.; Carlson, A.; Hein, M. Y.; Geiger, T.; Mann, M.; Cox, J. The Perseus Computational Platform for Comprehensive Analysis of (Prote)Omics Data. *Nat. Methods* **2016**, *13*, 731−740.
(35) Eklund, A. S.; Comberlato, A.; Parish, I. A.; Jungmann, R.; Bastings, M. M. C. Quantification of Strand Accessibility in Biostable DNA Origami with Single-Staple Resolution. *ACS Nano* **2021**, *15*, 17668−17677.
(36) Bastings, M. M. C.; Anastassacos, F. M.; Ponnuswamy, N.; Leifer, F. G.; Cuneo, G.; Lin, C.; Ingber, D. E.; Ryu, J. H.; Shih, W. M. Modulation of the Cellular Uptake of DNA Origami through Control over Mass and Shape. *Nano Lett.* **2018**, *18*, 3557−3564.
(37) Pinals, R. L.; Chio, L.; Ledesma, F.; Landry, M. P. Engineering at the Nano-Bio Interface: Harnessing the Protein Corona Towards Nanoparticle Design and Function. *Analyst* **2020**, *145*, 5090−5112.
(38) Walkey, C. D.; Olsen, J. B.; Guo, H.; Emili, A.; Chan, W. C. W. Nanoparticle Size and Surface Chemistry Determine Serum Protein Adsorption and Macrophage Uptake. *J. Am. Chem. Soc.* **2012**, *134*, 2139−2147.
(39) Li, M.; Jiang, S.; Simon, J.; Paßlick, D.; Frey, M.-L.; Wagner, M.; Mailänder, V.; Crespy, D.; Landfester, K. Brush Conformation of Polyethylene Glycol Determines the Stealth Effect of Nanocarriers in the Low Protein Adsorption Regime. *Nano Lett.* **2021**, *21*, 1591−1598.

(40) Morzy, D.; Tekin, C.; Caroprese, V.; Rubio-Sánchez, R.; Di Michele, L.; Bastings, M. M. C. Interplay of the Mechanical and Structural Properties of DNA Nanostructures Determines Their Electrostatic Interactions with Lipid Membranes. *Nanoscale* **2023**, *15*, 2849−2859.
(41) Santana, M. A.; Pedraza-Alva, G.; Olivares-Zavaleta, N.; Madrid-Marina, V.; Horejsi, V.; Burakoff, S. J.; Rosenstein, Y. CD43-mediated Signals Induce DNA Binding Activity of AP-1, NF-AT, and NFκB Transcription Factors in Human T Lymphocytes. *J. Biol. Chem.* **2000**, *275*, 31460−31468.
(42) Hirata, F.; Corcoran, G. B.; Hirata, A.; Hirata, F.; Corcoran, G. B.; Hirata, A. *Mono-Ubiquitination of Nuclear Annexin A1 and Mutagenesis*; IntechOpen, 2012.
(43) Guschina, T. A.; Soboleva, S. E.; Nevinsky, G. A. Recognition of Specific and Nonspecific DNA by Human Lactoferrin. *J. Mol. Recognit.* **2013**, *26*, 136−148.
(44) He, J.; Furmanski, P. Sequence Specificity and Transcriptional Activation in the Binding of Lactoferrin to DNA. *Nature* **1995**, *373*, 721−724.
(45) Soboleva, S. E.; Sedykh, S. E.; Alinovskaya, L. I.; Buneva, V. N.; Nevinsky, G. A. Cow Milk Lactoferrin Possesses Several Catalytic Activities. *Biomolecules* **2019**, *9*, 208.
(46) Zhou, L.; Chen, H.-M.; Qu, S.; Li, L.; Zhao, W.; Liang, Z.-G.; Yu, B.-B.; Chen, K.-H.; Lu, Q.-T.; Lin, G.-X.; Zhu, X.-D. Reduced QSOX1 Enhances Radioresistance in Nasopharyngeal Carcinoma. *Oncotarget* **2017**, *9*, 3230−3241.
(47) Elfenbein, A.; Simons, M. Syndecan-4 Signaling at a Glance. *J. Cell Sci.* **2013**, *126*, 3799.
(48) Kim, H.; Röth, D.; Isoe, Y.; Hayashi, K.; Mochizuki, C.; Kalkum, M.; Nakamura, M. Protein Corona Components of Polyethylene Glycol-Conjugated Organosilica Nanoparticles Modulates Macrophage Uptake. *Colloids Surf., B* **2021**, *199*, 111527.
(49) Dunkelberger, J. R.; Song, W.-C. Complement and Its Role in Innate and Adaptive Immune Responses. *Cell Res.* **2010**, *20*, 34−50.
(50) Lundqvist, M.; Stigler, J.; Cedervall, T.; Berggård, T.; Flanagan, M. B.; Lynch, I.; Elia, G.; Dawson, K. The Evolution of the Protein Corona around Nanoparticles: A Test Study. *ACS Nano* **2011**, *5*, 7503−7509.
(51) Kokkinopoulou, M.; Simon, J.; Landfester, K.; Mailänder, V.; Lieberwirth, I. Visualization of the Protein Corona: Towards a Biomolecular Understanding of Nanoparticle-Cell-Interactions. *Nanoscale* **2017**, *9*, 8858−8870.
(52) Li, S.; Ju, Y.; Zhou, J.; Faria, M.; Ang, C.-S.; Mitchell, A. J.; Zhong, Q.-Z.; Zheng, T.; Kent, S. J.; Caruso, F. Protein Precoating Modulates Biomolecular Coronas and Nanocapsule−Immune Cell Interactions in Human Blood. *J. Mater. Chem. B* **2022**, *10*, 7607−7621.
(53) Cunin, P.; Beauvillain, C.; Miot, C.; Augusto, J.-F.; Preisser, L.; Blanchard, S.; Pignon, P.; Scotet, M.; Garo, E.; Fremaux, I.; Chevailler, A.; Subra, J.-F.; Blanco, P.; Wilson, M. R.; Jeannin, P.; Delneste, Y. Clusterin Facilitates Apoptotic Cell Clearance and Prevents Apoptotic Cell-Induced Autoimmune Responses. *Cell Death Dis.* **2016**, *7*, No. e2215.
(54) Bartl, M. M.; Luckenbach, T.; Bergner, O.; Ullrich, O.; Koch-Brandt, C. Multiple Receptors Mediate ApoJ-Dependent Clearance of Cellular Debris into Nonprofessional Phagocytes. *Exp. Cell Res.* **2001**, *271*, 130−141.
(55) Najer, A.; Rifaie-Graham, O.; Yeow, J.; Adrianus, C.; Chami, M.; Stevens, M. M. Differences in Human Plasma Protein Interactions between Various Polymersomes and Stealth Liposomes as Observed by Fluorescence Correlation Spectroscopy. *Macromol. Biosci.* **2022**, 2200424.

NOTE ADDED AFTER ASAP PUBLICATION

This paper was published ASAP on June 7, 2023, with an error in the title. The corrected version was reposted June 7, 2023.

https://doi.org/10.1021/acspolymersau.3c00009
ACS Polym. Au 2023, 3, 344−353